HHS Public Access

Author manuscript

Bioorg Med Chem Lett. Author manuscript; available in PMC 2016 January 12.

Published in final edited form as:

Bioorg Med Chem Lett. 2013 December 1; 23(23): 6350–6354. doi:10.1016/j.bmcl.2013.09.074.

Novel Cancer-Targeting SPECT/NIRF Dual-modality Imaging Probe ^{99m}Tc -PC-1007: Synthesis and Biological Evaluation

Yi Zhang[a,§], **Li Xiao**[a,§], **Kosta Popovic**[a], **Xiuzhen Xie**[a,#], **Mahendra D. Chordia**[a], **Leland W.K. Chung**[b], **Mark B. Williams**[a], **Wei Yue**[c], and **Dongfeng Pan**[a,*]

[a]Department of Radiology and Medical Imaging, University of Virginia, Charlottesville, VA 22908, USA

[b]Uro-Oncology Research, Samuel Oschin Comprehensive Cancer Institute, Cedars-Sinai Medical Center, Los Angeles, California 90048, USA

[c]Department of Endocrinology and Metabolism, University of Virginia, Charlottesville, VA 22908, USA

Abstract

Synthesis, characterization, *in vitro* and *in vivo* biological evaluation of a heptamethine cyanine based dual-mode single-photon emission computed tomography (SPECT)/near infrared fluorescence (NIRF) imaging probe ^{99m}Tc-PC-1007 is described. ^{99m}Tc-PC-1007 exhibited preferential accumulation in human breast cancer MCF-7 cells. Cancer-specific SPECT/CT and NIRF imaging of ^{99m}Tc -PC-1007 was performed in a breast cancer xenograft model. The probe uptake ratio of tumor to control (spinal cord) was calculated to be 4.02 ± 0.56 at 6 h post injection (pi) and 8.50 ± 1.41 at 20 h pi ($P<0.0001$). Pharmacokinetic parameters such as blood clearance and organ distribution were assessed.

Keywords

Breast cancer; dual-modality; heptamethine cyanine dye; SPECT; 99m-Technetium; near infrared fluorescence

Cancer is a dynamically intricate and only partially understood disease affecting many balanced biological processes required for normal cell growth and cell division. Early diagnosis of cancer is a key factor that defines prognosis which ultimately reflects in prolonged survival of patients[1,2]. Compared with other techniques such as magnetic resonance (MR)[3], Ultrasound (US)[4], high sensitivity of nuclear imaging (PET/SPECT)[5,6] may offer better solution for detection and diagnosis of cancer at early stages and for

*Corresponding author: Dongfeng Pan, PhD, Department of Radiology and Medical Imaging, University of Virginia, Rm 263, 480 Ray C. Hunt Drive, Snyder Building, Charlottesville, VA, 22908, Phone: (434) 243-2893; Fax: (434) 924-9435; dp3r@virginia.edu.

§These authors contributed equally to this work

#Current address: College of Life Science, Hainan Normal University, Haikou, 571158, P.R. of China

monitoring the therapeutic response later in treatments[7-9]. Nuclear imaging probes such as 2-Deoxy-2-(^{18}F)fluoro-D-glucose (FDG)[10,11], (^{18}F)Fluoro-3-deoxy-3-L-fluorothymidine (FLT)[12,13] being functional agents have been widely used in research and in clinic for cancer diagnostic imaging, as well as for monitoring the progress in treatment. However, FDG exhibits poor specificity and is a metabolic tracer, while FLT is more cancer specific but less sensitive due to its limited incorporation in the DNA of cancer cells prohibiting their widespread utility in the early detection and diagnosis of cancer[14,15]. Therefore novel nuclear imaging probes with high sensitivity, cancer-targeting specificity and optimized physiochemical properties are desirable. The most ideal cancer imaging probe would be adaptable to a broad range of cancer types, amenable to easy synthesis, sensitive enough for detection and diagnosis, cost effective and potentially feasible for monitoring treatment effect[16].

We recently reported a new heptamethine cyanine dye based PET/near-infrared fluorescence (NIRF) probe ^{64}Cu-PC-1001 for dual-mode cancer imaging[17]. In our construct, the heptamethine cyanine dye was employed as cancer-specific carrier due to its inherent targeting property of a broad spectrum of cancer cell lines and tumors[18-21]. However, application of PET imaging in research and clinical settings may be confined by the high cost and limited supply of cyclotron-produced ^{64}Cu radioisotope. In contrast, ^{99m}Tc version of imaging probe for single photon gamma emission computed tomography (SPECT) imaging provides a smart alternative due to the abundant availability and lower cost of ^{99m}Tc isotope as well as imaging modality[22-25]. In an effort to broaden application of the cancer-specific cyanine dye in SPECT, we sought to synthesize and evaluate a ^{99m}Tc labeled probe ^{99m}Tc-PC-1007 for imaging of cancer in dual-modality (SPECT/NIRF).

The cancer-targeting carrier heptamethine cyanine dye (MHI-148) **5** was synthesized following previously reported procedures[26] (Supplemental Scheme 1). As shown in Scheme 1, one of the two carboxyl group of 3H-indolenines of **5** was functionalized to NHS-ester, conjugated with N$^{\alpha}$-*t*-Boc-protected lysine, and followed by deprotection of *t*-Boc with TFA yielded MHI-148-Lysine conjugate **7**. Conjugate **7** was purified by reverse phase semi-preparative HPLC[27] and characterized thoroughly by ^{1}H, ^{13}C NMR, mass analysis [m/z 811 (M^{+})][28] and fluorescence spectroscopy (Supplemental Figure 1-4). Purified conjugate **7** was then mixed with *t*-Boc-HYNIC-OSu, followed by TFA deprotection, yielding the precursor MHI-HYNIC **8**. Compound **8** was purified by semi-preparative HPLC[27] (Supplemental Figure 5) and characterized by ^{1}H-NMR and mass analysis [m/z 946.6 (M^{+})][29] prior to radio-metal complexation (Supplemental Figure 6-7). The radiolabeled ^{99m}Tc-PC-1007 was obtained by performing standard metalation of **8** with [^{99m}Tc]pertechnetate ($Na^{99m}TcO_4$, Cardinal Health Inc. Charlottesville, VA) in the presence of nicotinic acid and tricine as co-ligands under stannous chloride mediated reducing conditions. The radiolabeled probe ^{99m}Tc-PC-1007 was purified from unlabeled precursors, other reagents and byproducts by semi-preparative HPLC[27] with radiochemical yield >80% (starting from 1.1 GBq of $^{99m}TcO_4^-$ to 888 MBq of labeled probe) and radiochemical purity of >95% (Supplemental Figure 8). Partition coefficient (log *P*) of probe ^{99m}Tc-PC-1007 was quantified by measuring distribution of radioactivity in octanol and water and calculated to be 1.03 ± 0.01. *In vitro* stability studies of ^{99m}Tc-PC-1007 was conducted by incubating the

probe with fetal bovine serum and followed by radio-HPLC analysis. ^{99m}Tc-PC-1007 appeared to be slowly decomposing in serum. Most of the probe was observed to be stable up to 6 hours in serum and displayed no appreciable degradation at earlier time points (1 and 3 hours, Supplemental Figure 9).

Time, concentration and organic anion transport polypeptides (OATPs) dependent cell uptake studies of ^{99m}Tc-PC-1007 were performed in human breast cancer MCF-7 cells. The cancer cell uptake in the initial 15-20 minutes was exponential and somewhat slowed down by 25-30 minutes (Figure 1a). In a similar fashion, the uptake was appreciable when probe concentration is less than 2 μM and reached a plateau beyond that concentration (Figure 1b). Cancer cell specific uptake was observed to be mediated by OATPs expressed on cancer cells as reported previously[17,18]. When MCF-7 cells were pre-treated with an OATP inhibitor bromosulfophthalein (BSP) (250 μM) and subsequently incubated with probe ^{99m}Tc-PC-1007, the resulting uptake was observed to be suppressed by ∼66% (Figure 1c). Significant difference in uptake of ^{99m}Tc-PC-1007 via fluorescence intensity between BSP-free and BSP-treated cancer cells also supported the observation that the OATP-mediated mechanism is at least partly responsible for cellular accumulation at microscopic level (Figure 1d). Similar trend and observations were made for PET imaging probe Cu64-PC-1001 from our lab previously[17].

MCF-7 cells grown in nude mice have long been used in our laboratory to evaluate the effects of estradiol, anti-estrogen, and other agents on tumor growth[30-33]. This xenograft model was used for all in vivo studies in accordance with current National Institutes of Health (NIH) guidelines and protocols that were approved by the University of Virginia Animal Care and Use Committee (ACUC). Mice were under anesthesia (1%-2% isoflurane in oxygen) throughout all imaging procedures. Four weeks after MCF-7 inoculation, probe ^{99m}Tc-PC-1007 (37 MBq, 200 μL saline) was injected into mice (n=3) via tail vein. MicroSPECT/CT imaging was performed at 6 h and 24 h post injection (pi) with custom-built scanner[34] (see Supplemental Materials for details). After each SPECT/CT scan, the mouse was transferred to the IVIS spectrum (Caliper Life Science, MA) for NIRF imaging with a filter set of *Excitation/Emission* = 745/820 nm (see Supplemental Materials). Representative in vivo fluorescence and SPECT/CT imaging of tumor bearing mice at 6 h and 20 h pi are presented in Figure 2a-d. Four tumors on ventral side were clearly visualized by fluorescence imaging at both 6 h and 20 h pi (Figure 2a). Preferential uptake and accumulation of ^{99m}Tc-PC-1007 in tumor regions (yellow dotted lined areas) was observed by SPECT, CT and co-registered SPECT/CT images at both time points (Figure 2b-d). To further quantify SPECT images, the spinal cord (Area 2 in Figure 2e) of transaxial slices was defined as background, to which the accumulated radioactivity in tumor region (Area 1 in Figure 2e) was normalized. The radioactivity ratio of tumor to spinal cord (Area 1/Area 2) was calculated to be 4.02 ± 0.56 at 6 h pi and 8.50 ± 1.41 at 20 h pi ($P<0.0001$) (Figure 2f). The favorable imaging profile of ^{99m}Tc-PC-1007 at later time point (20 h pi) may be due to the slow elimination of the probe from blood. The detailed imaging of transaxial, coronal and sagital slices is presented in Supplemental Figure 10 and 11 for 6 and 20h pi respectively. The quantitative comparison between NIR signal and radio signal could not be

performed as reported earlier[17] but the similar trend of probe uptake was observed over time.

Blood clearance study of ^{99m}Tc-PC-1007 was performed in tumor-bearing nude mice (*n=4*) to determine related pharmacokinetic properties (see Supplemental Materials). The rate of clearance from blood in first 300 minutes was observed to be very fast, but slowed down considerably beyond 300 minutes. The data was fitted to a mono-exponential decay equation $y = y_0 + A_1 \times \exp[-(x-x_0)/t_1]$, and the blood half-life ($T_{1/2}$) was calculated to be 169 ± 26 minutes using GraphPad Prism (Figure 3a). Ex vivo biodistribution studies were carried out to examine the uptake profile of ^{99m}Tc -PC-1007 in tumors, organs and tissues. At 6h pi, ^{99m}Tc-PC-1007 showed the highest retention in blood (2.80 ± 0.11%ID/g) and moderate accumulation in tumor (0.56 ± 0.05%ID/g), stomach (0.63 ± 0.08%ID/g), lung (0.71 ± 0.14%ID/g), liver (0.62 ± 0.08%ID/g), heart (0.63 ± 0.1%ID/g) and kidney (0.79 ± 0.06%ID/g) while other organs demonstrated relative low levels of uptake (<0.50%ID/g). At 27 h pi, despite the highest retention was still observed in blood (1.53 ± 0.12%ID/g), the tumor uptake have been significantly improved as indicated by the ratio of tumor to blood (T/B). The T/B ratio increased from 0.20 to 0.36 from 6 h pi to 27 h pi respectively (Figure 3b). This approximate 81% increase in T/B ratio suggested that probe ^{99m}Tc -PC-1007 could be cleared out of blood slowly during one-day post injection while preferential tumor uptake and retention remained at a stable and relative high level during the imaging window (0.5-0.6%ID/g, highly comparable to the poor accumulation in other major organs, such as liver and kidney, which are responsible for metabolism). Meanwhile, probe binding study with blood components revealed that most of radioactivity (>95%) was associated with serum (Supplemental Figure 12). The binding of probes to serum may explain the slow clearance and high retention in the blood. Detailed procedures of all experiments are described in Supplemental Materials.

In conclusion, the cancer-targeting SPECT/NIRF dual-modality imaging probe ^{99m}Tc-PC-1007 has been successfully synthesized and characterized. The probe exhibited cancer-specific targeting and accumulation properties *in vitro* and *in vivo* experiments. Development of ^{99m}Tc-labeled “broad spectrum” cancer-targeting imaging probes would aid scientists in advancing anti-cancer drug discovery and assist clinicians in monitoring the efficacy of therapeutics. Further structural modifications to optimize tumor targeting are ongoing in our laboratory with the aim to deliver more efficient imaging at early time point, which may be realized by improving water solubility and lowering non-covalent hydrophobic binding of the probe to proteins in blood.

Supplementary Material

Refer to Web version on PubMed Central for supplementary material.

Acknowledgments

This research was supported by Nihon Medi Physics residual fund (MD-RADL Pan NMP RPZF001917E), private gift fund to DP, and NIH grant PO1CA098912 to LWKC. We are grateful to Dr. Ji-Ping Wang for animal care and handling.

References and notes

1. Etzioni R, Urban N, Ramsey S, McIntosh M, Schwartz S, Reid B, Radich J, Anderson G, Hartwell L. Nat Rev Cancer. 2003; 3:243–252. [PubMed: 12671663]
2. Fass L. Molecular Oncology. 2008; 2:115–152. [PubMed: 19383333]
3. Flacke S, Fischer S, Scott MJ, Fuhrhop RJ, Allen JS, McLean M, Winter P, Sicard GA, Gaffney PJ, Wickline SA, Lanza GM. Circulation. 2001; 104:1280–1285. [PubMed: 11551880]
4. Liang HD, Blomley MJK. British Journal of Radiology. 2003; 76:S140–S150. [PubMed: 15572336]
5. Ametamey SM, Honer M, Schubiger PA. Chemical Reviews. 2008; 108:1501–1516. [PubMed: 18426240]
6. Frangioni JV. Journal of Clinical Oncology. 2008; 26:4012–4021. [PubMed: 18711192]
7. Willmann JK, van Bruggen N, Dinkelborg LM, Gambhir SS. Nature Reviews Drug Discovery. 2008; 7:591–607. [PubMed: 18591980]
8. Weissleder R, Pittet MJ. Nature. 2008; 452:580–589. [PubMed: 18385732]
9. Blasberg RG. Molecular Cancer Therapeutics. 2003; 2:335–343. [PubMed: 12657729]
10. Kelloff GJ, Hoffman JM, Johnson B, Scher HI, Siegel BA, Cheng EY, Cheson BD, O'Shaughnessy J, Guyton KZ, Mankoff DA, Shankar L, Larson SM, Sigman CC, Schilsky RL, Sullivan DC. Clinical Cancer Research. 2005; 11:2785–2808. [PubMed: 15837727]
11. Quon A, Gambhir SS. Journal of Clinical Oncology. 2005; 23:1664–1673. [PubMed: 15755974]
12. Dimitrakopoulou-Strauss A, Strauss LG. European Journal of Nuclear Medicine and Molecular Imaging. 2008; 35:523–526. [PubMed: 18183395]
13. Barthel H, Cleij MC, Collingridge DR, Hutchinson OC, Osman S, He QM, Luthra SK, Brady F, Price PM, Aboagye EO. Cancer Research. 2003; 63:3791–3798. [PubMed: 12839975]
14. Shreve PD, Anzai Y, Wahl RL. Radiographics. 1999; 19:61–77. [PubMed: 9925392]
15. Abouzied MM, Crawford ES, Nabi HA. Journal of Nuclear Medicine Technology. 2005; 33:145–155. [PubMed: 16145222]
16. Joshi BP, Wang TD. Cancers. 2010; 2:1251–1287. [PubMed: 22180839]
17. Xiao L, Zhang Y, Yue W, Xie X, Wang Jp, Chordia MD, Chung LWK, Pan D. Nuclear Medicine and Biology. 2013; 40:351–360. [PubMed: 23375364]
18. Yang X, Shi C, Tong R, Qian W, Zhau HE, Wang R, Zhu G, Cheng J, Yang VW, Cheng T, Henary M, Strekowski L, Chung LWK. Clinical Cancer Research. 2010; 16:2833–2844. [PubMed: 20410058]
19. Yang XS, Wang C, Chu R, Hu C, Master P, Osunkoya V, Kim AO, Zhau HL, Chung HE, L LK. The Journal of Urology. 2013 In press.
20. Zhang C, Liu T, Su YP, Luo SL, Zhu Y, Tan X, Fan S, Zhang LL, Zhou Y, Cheng TM, Shi CM. Biomaterials. 2010; 31:6612–6617. [PubMed: 20542559]
21. Luo SL, Zhang EL, Su YP, Cheng TM, Shi CM. Biomaterials. 2011; 32:7127–7138. [PubMed: 21724249]
22. Zhang Y, Xiao L, Chordia MD, Locke LW, Williams MB, Berr SS, Pan D. Bioconjugate Chemistry. 2010; 21:1788–1793. [PubMed: 20843030]
23. Rahmim A, Zaidi H. Nuclear Medicine Communications. 2008; 29:193–207. 10.1097/MNM.0b013e3282f3a515. [PubMed: 18349789]
24. Jansen FP, Vanderheyden JL. Nuclear Medicine and Biology. 2007; 34:733–735. [PubMed: 17921025]
25. Gholamrezanejhad A, Mirpour S, Mariani G. Journal of Nuclear Medicine. 2009; 50:16N–18N.
26. Narayanan N, Patonay G. Journal of Organic Chemistry. 1995; 60:2391–2395.
27. HPLC condition: Semi-preparative reversed-phase high-performance liquid chromatography (RP-HPLC) was performed with an Apollo C18 reversed-phase column (5m, 250×10mm) on a Varian system with ABI Spectroflow 783 UV detector and Bioscan NaI solid scintillation Flow Count Radio-HPLC detector. The mobile phase was changed from 30% Solvent A (0.1% TFA in water) and 70% Solvent B (0.1% TFA in 80% aqueous acetonitrile) to 100% Solvent B at 30 minutes at a flow rate of 3 mL/min.

28. Characterization of compound **7**: ^{1}H NMR for **7** (300 MHz, DMSO-d_6): δ 1.2-1.45 (m, CH_2), 1.47-1.60 (m, CH_2), 1.67 (s, 12H. CH_3), 1.60-1.95 (m, 1H), 2.05 (t, J=9.0 Hz, 2H), 2.21 (t, J=9.0 Hz, 2H), 2.71 (m, 4H), 2.97 (m, 2H), 3.86 (m, 1H, N-CH), 4.21 (4H, brs, NH_2, COOH), 6.30 and 6.35 (brs, 2H, olefinic), 7.20-7.35 (m, 2H, ArH), 7.35 – 7.50 (m, 3H, ArH), 7.60 - 7.75 (m, Ar H), 7.81 (m, ArH), 8.25-8.45 (m, ArH). ^{13}C NMR (DMSO-d_6): δ 21.8, 24.2, 25.7, 25.8, 27.5, 28.7, 33.5, 49.0, 51.9, 101.6, 111.6, 113.9, 117.8, 121.7, 122.5, 125.2, 126.2, 128.7, 141.1, 142.1, 143.0, 146.1, 157.7, 158.2, 158.7, 159.1, 171.1, 171.8, 172.3, 178.3. Mass: observed m/z 811 $(M)^+$ for $C_{48}H_{64}ClN_4O_5$ expected m/z 811.

29. Characterization of precursor **8:** ^{1}H NMR for **8** (300 MHz, DMSO-d_6): δ 1.2-1.45 (m), 1.47-1.60 (m), 1.67 (s, 12H. CH_3), 1.60-1.95 (m, 1H), 2.05 (t, J=9.0 Hz, 2H), 2.21 (t, J=9.0 Hz, 2H), 2.71 (m, 4H), 2.97 (m, 2H), 3.86 (m, 1H, N-CH), 4.21 (4H, brs, NH_2 COOH), 6.30 and 6.35 (brs, 2H, olefinic), 7.20-7.35 (m, 2H, ArH), 7.35 – 7.50 (m, 3H, ArH), 7.60 - 7.75 (m, Ar H), 7.81 (m, ArH), 8.25-8.45 (m, ArH). Mass analysis: observed m/z 946.6 $(M)^+$ for $C_{54}H_{69}ClN_7O_6$ expected m/z 946.5 and m/z 960.7 $(M+Na)^+$ for $C_{54}H_{68}ClN_7O_6Na$.

30. Santen RJ, Lobenhofer EK, Afshari CA, Bao Y, Song RX. Breast Cancer Research and Treatment. 2005; 94:213–223. [PubMed: 16258703]

31. Yue W, Wang JP, Conaway M, Masamura S, Li Y, Santen RJ. Endocrinology. 2002; 143:3221–3229. [PubMed: 12193533]

32. Lehnes K, Winder AD, Alfonso C, Kasid N, Simoneaux M, Summe H, Morgan E, Iann MC, Duncan J, Eagan M, Tavaluc R, Evans CH, Russell R, Wang A, Hu F, Stoica A. Endocrinology. 2007; 148:1171–1180. [PubMed: 17138652]

33. Peng CY, Fong PC, Yu CC, Tsai WC, Tzeng YM, Chang WW. Molecules. 2013; 18:2539–2548. [PubMed: 23442930]

34. Kundu BK, Stolin AV, Pole J, Baumgart L, Fontaine M, Wojcik R, Kross B, Zorn C, Majewski S, Williams MB. Ieee Transactions on Nuclear Science. 2006; 53:66–70.

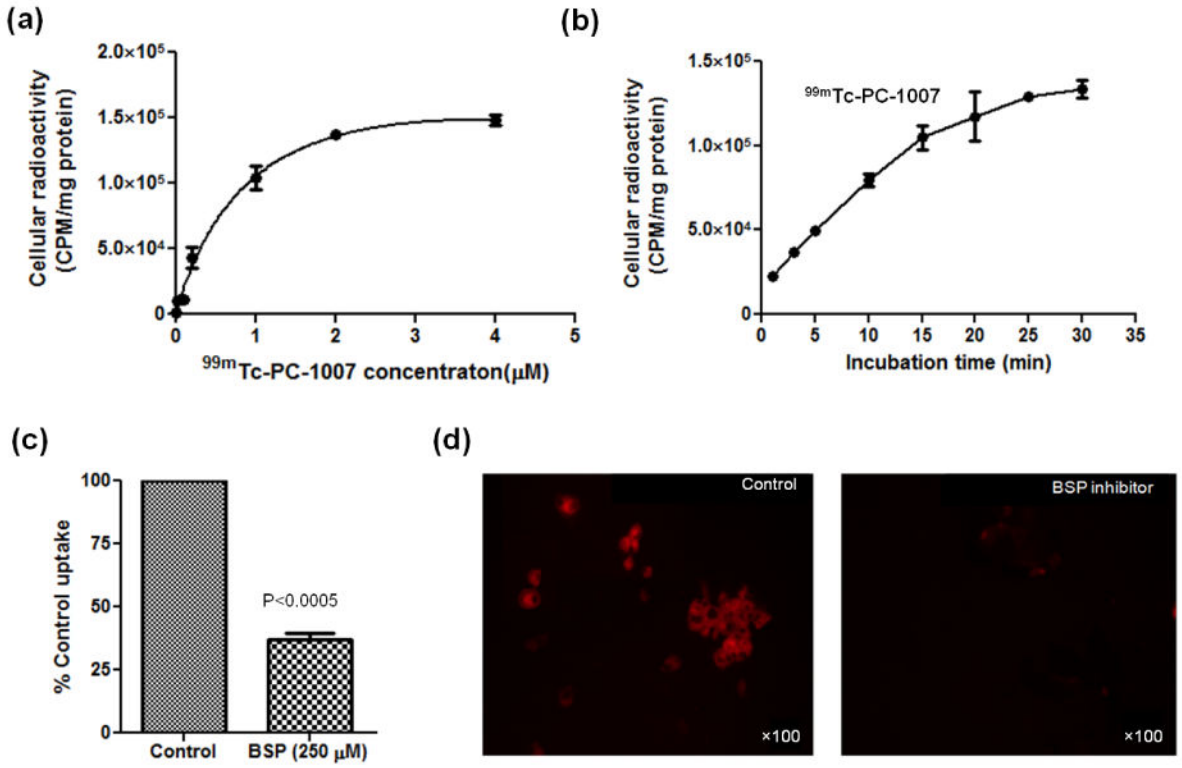

Figure 1.

In vitro cell uptake of ^{99m}Tc-PC-1007 in MCF-7 breast cancer cell lines. (a) Concentration-dependent cell uptake plotted as cellular radioactivity (CPM/mg protein) vs. probe concentration (μM). (b) Time-dependent cell uptake plotted as cellular radioactivity (CPM/mg protein) vs. incubation time (min). (c) Normalized %cell uptake in the absence and presence of an OATP inhibitor, bromosulfophthalein (BSP) (250 μM), supporting the transporter-mediated cell uptake mechanism. (d) Fluorescence microscopic imaging of MCF-7 cells upon accumulation of ^{99m}Tc-PC-1007 with or without BSP (250 μM) at 100 fold magnification (shown as ×100 on images).

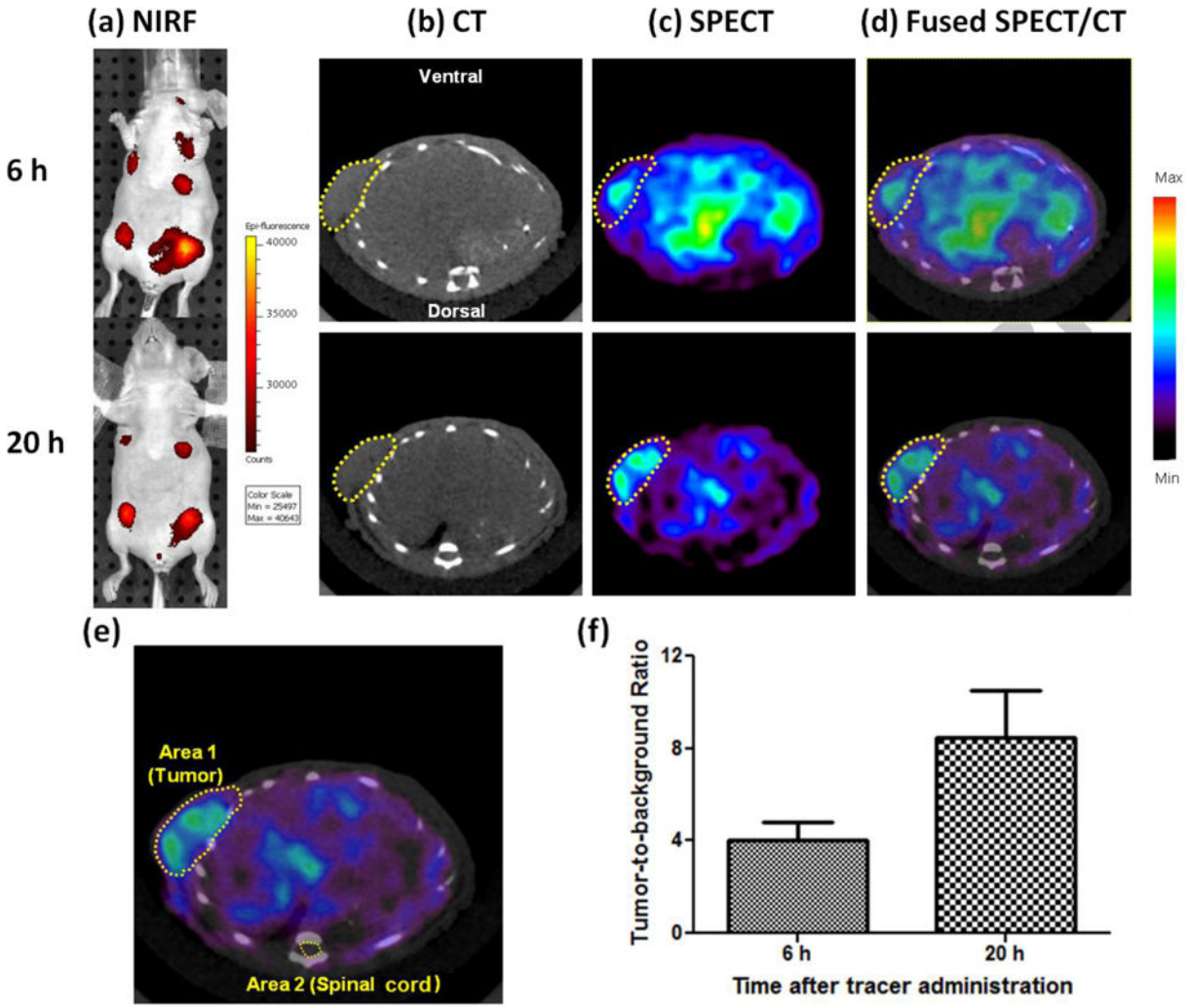

Figure 2.

Representative in vivo SPECT/CT and NIRF imaging of probe ^{99m}Tc-PC-1007. (a) Epi-fluorescence imaging of tumor-bearing mice at 6h and 20 h pi. (b) Transaxial CT, (c) SPECT and (d) fused SPECT/CT images of ^{99m}Tc-PC-1007 at 6h and 20 h pi. (e) Example of ROI measurement of Area 1 (Tumor) and Area 2 (Spinal cord as background) on a typical transaxial SPECT/CT image. (f) Tumor-to-background ratios calculated as ratio of accumulated radioactivity in designated areas (n=3 per time point). Note: tumors are indicated by yellow dotted circles on all images.

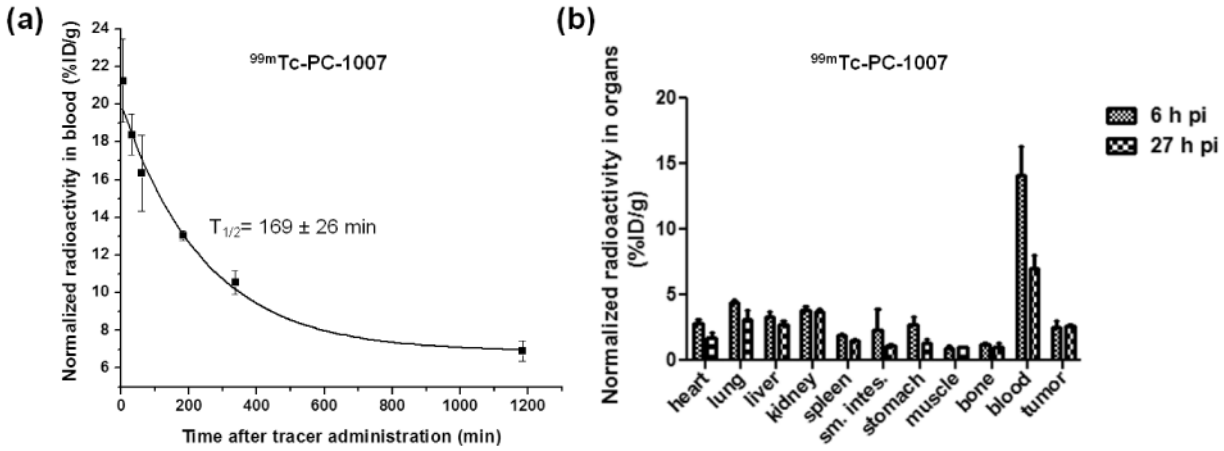

Figure 3.

Pharmacokinetic profile of probe ^{99m}Tc-PC-1007. (a) Monoexponential blood clearance curve of ^{99m}Tc-PC-1007 in tumor-bearing nude mice (*n=4*) after probe administration via tail vein. The calculated half-life in blood was observed to be 169 ± 26 minutes when fitted into the equation: $y = y_0 + A_1 \times \exp[-(x-x_0)/t_1]$. (b) Ex vivo organ distribution of ^{99m}Tc-PC-1007 at 6 h and 27 h pi, revealing long circulation of probe in blood and relatively high accumulation in tumor, lung, liver and kidney.

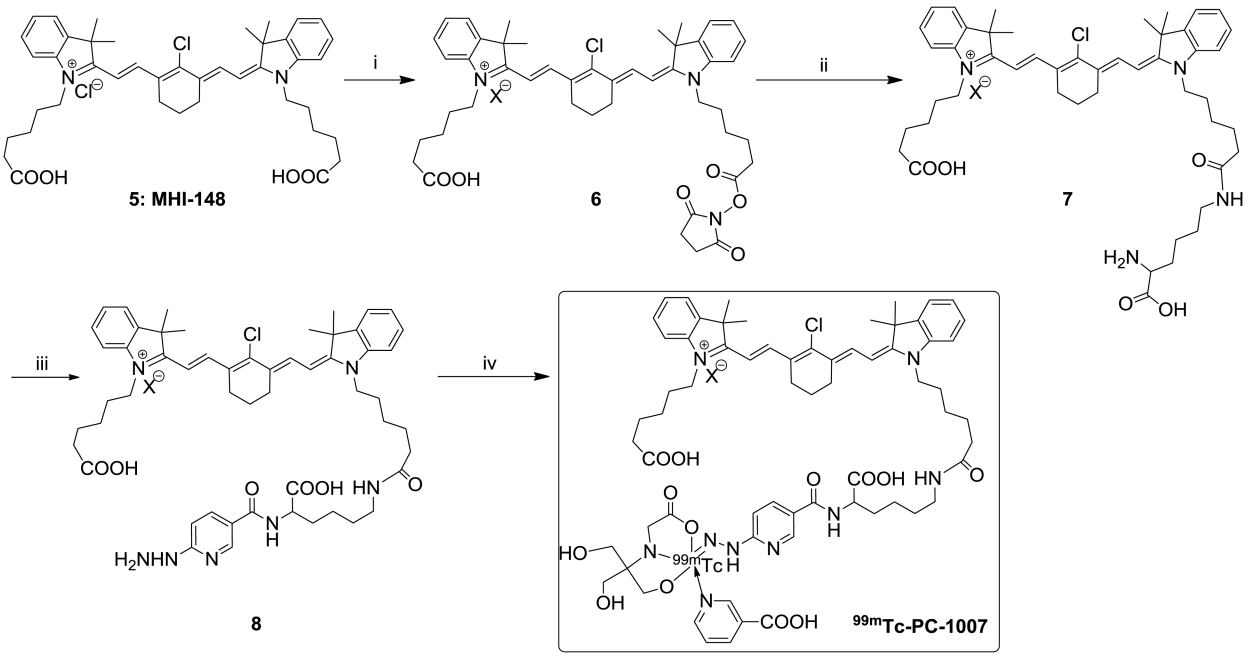

Scheme 1.

Synthesis of ^{99m}Tc -PC-1007. Reagents and conditions: (i) N-hydroxy succinimide, DCC, anhydrous CH_2Cl_2, rt; (ii) a. *N*-α-Boc-L-Lysine, borate buffer, pH 8.5, 4°C; b. TFA, 45%; (iii) a. Boc-HYNIC-OSu, borate buffer, pH 8.5, 4°C; b. TFA, 72%; (iv) $Na^{99m}TcO_4$, $SnCl_2$, Nicotinic acid, tricine, >80%.